Interplay between N-WASP and CK2 optimizes clathrin-mediated endocytosis of EGFR

Magda Galovic[1], Dalu Xu[2], Liliana Beatriz Areces[3], Rob van der Kammen[1] and Metello Innocenti[1,*]

[1]The Netherlands Cancer Institute (NKI), Plesmanlaan 121, 1066 CX Amsterdam, The Netherlands
[2]Institute of Biochemistry II, Goethe University Medical School, Theodor-Stern-Kai 7, D-60590 Frankfurt, Germany
[3]European Institute of Oncology, Via Ripamonti 435, 20141 Milan, Italy
*Author for correspondence (m.innocenti@nki.nl)

Accepted 9 March 2011
Journal of Cell Science 124, 2001-2012

doi:10.1242/jcs.081182

Summary

Clathrin-mediated endocytosis (CME) involves spatially and temporally restricted molecular dynamics, to which protein kinases and actin contribute. However, whether and how these two elements merge to properly execute CME remains unknown. Here, we show that neural Wiskott–Aldrich syndrome protein (N-WASP) and casein kinase 2 (CK2) form a complex and localize to clathrin-coated vesicles. N-WASP binds to and is phosphorylated by CK2, thereby reducing the kinase activity of CK2. By contrast, N-WASP-promoted actin polymerization is decreased upon both phosphorylation and binding of CK2. Knockdown of CK2 and N-WASP, either alone or in combination, causes a similar inhibition in the initial rate of CME of epidermal growth factor receptor (EGFR) and its accumulation at the plasma membrane. Increased levels of EGFR at the cell surface can only be efficiently rescued by reconstituting the N-WASP–CK2 complex with either wild-type or phosphorylation-mimicking N-WASP and wild-type CK2. Notably, perturbation of N-WASP–CK2 complex function showed that N-WASP controls the presence of F-actin at clathrin-coated structures. In summary, the N-WASP–CK2 complex integrates in a single circuit different activities contributing to CME.

Key words: N-WASP, CK2, Endocytosis, Actin cytoskeleton

Introduction

Recruitment and concentration of cargos into clathrin-coated structures (CCSs) on the plasma membrane and selective receptor-mediated uptake of nutrients and signalling molecules are hallmarks of clathrin-mediated endocytosis (CME) in mammalian cells (Conner and Schmid, 2003). Clathrin, AP-2 and several other cytosolic proteins combine in a multi-layered membrane-scaffolding structure referred to as the vesicle coat, whose incessant remodelling controls clathrin-coated pit (CCP) size and shape (Ehrlich et al., 2004; Kirchhausen, 2000). These rearrangements are crucial for the efficient completion of single endocytic events, which ultimately result in fission and formation of clathrin-coated vesicles (CCVs) (Ungewickell and Hinrichsen, 2007). Coat-associated machineries are required to modify the functional and structural properties of coat components and to generate force throughout CCV biogenesis. Not surprisingly, reversible phosphorylation of endocytic proteins (Conner and Schmid, 2003; Korolchuk and Banting, 2003; Ungewickell and Hinrichsen, 2007) and actin dynamics (Kaksonen et al., 2006; Perrais and Merrifield, 2005) are believed to be important to properly execute CME.

Casein kinase 2 (CK2) is a major serine/threonine kinase associated with brain-derived CCVs (Bar-Zvi and Branton, 1986; Korolchuk and Banting, 2002). The regulatory and catalytic subunits of CK2 (β and α and/or α′, respectively) exist as either free subunits or a holoenzyme composed of two regulatory and two catalytic subunits (Bibby and Litchfield, 2005). The CK2 tetramer, as well as isolated subunits, localize both in the nucleus and cytoplasm (Meggio and Pinna, 2003). Although CK2 is constitutively active (Arrigoni et al., 2008; Korolchuk and Banting, 2003; Meggio and Pinna, 2003), its activity might be repressed on coated vesicles (Korolchuk and Banting, 2002).

Neural Wiskott–Aldrich syndrome protein (N-WASP) is a member of the WASP and WAVE family of nucleation-promoting factor (NPF) proteins, characterized by a C-terminal VCA (for verprolin homology domain, cofilin homology domain and acidic domain) region that binds to and activates the Arp2/3 complex (Takenawa and Suetsugu, 2007). An intramolecular interaction between the VCA and the N-terminal basic region (B)–GTPase-binding domain (GBD) module prevents VCA–Arp2/3 complex formation, thus locking N-WASP in an inhibited conformation. Proteins associating with either the B-GBD or the P-rich (proline-rich) region (Takenawa and Suetsugu, 2007), or mimicking the C domain of the VCA region (Cheng et al., 2008; Sallee et al., 2008), employ different mechanisms to unlock N-WASP. N-WASP removal impairs CME of epidermal growth factor receptor (EGFR) in both human and murine cells (Benesch et al., 2005; Innocenti et al., 2005). Although actin is not strictly essential for CME, it is required for the biogenesis of at least a subset of CCVs, on which N-WASP, cortactin and the Arp2/3 complex association peaks just before fission (Benesch et al., 2005; Ferguson et al., 2009; Innocenti et al., 2005; Lamaze et al., 1997; Merrifield et al., 2005; Merrifield et al., 2004; Yarar et al., 2005). Interestingly, N-WASP is present in low amounts from the early stages of CCP maturation (Merrifield et al., 2004; Perrais and Merrifield, 2005), suggesting that it has multiple roles in this process.

Despite this information, whether and how kinase and actin functions are integrated during CME remains unknown. We find that N-WASP and CK2 enter into a complex that controls CME and cell-surface distribution of EGFR. Interplay between N-WASP and CK2 activities regulates actin-based CME and requires the ability of both proteins to dynamically assemble in a complex. We conclude that the N-WASP–CK2 complex integrates kinase and actin-polymerizing machineries into a single molecular circuit optimizing CME.

Journal of Cell Science

Results

N-WASP and CK2 form a complex and localize onto CCVs

Matrix-assisted laser-desorption ionization–time-of-flight mass spectrometry (MALDI–TOF-MS) analysis identified endogenous CK2α as a protein specifically co-precipitating with Flag-tagged full-length N-WASP in HEK-293T cells (data not shown). This interaction was validated by immunoblotting with anti-CK2α antibodies (Fig. 1A). Next, we investigated whether endogenous N-WASP and CK2 form a complex using an anti-N-WASP antiserum (supplementary material Fig. S1A). Immunoprecipitation studies revealed that all CK2 subunits interact in an EGF-insensitive manner with N-WASP in HeLa cells (Fig. 1B). Similar observations were made in HEK-293T and COS-7 cells (data not shown). Size-exclusion chromatography showed partial coelution of N-WASP and CK2 (supplementary material Fig. S1B).

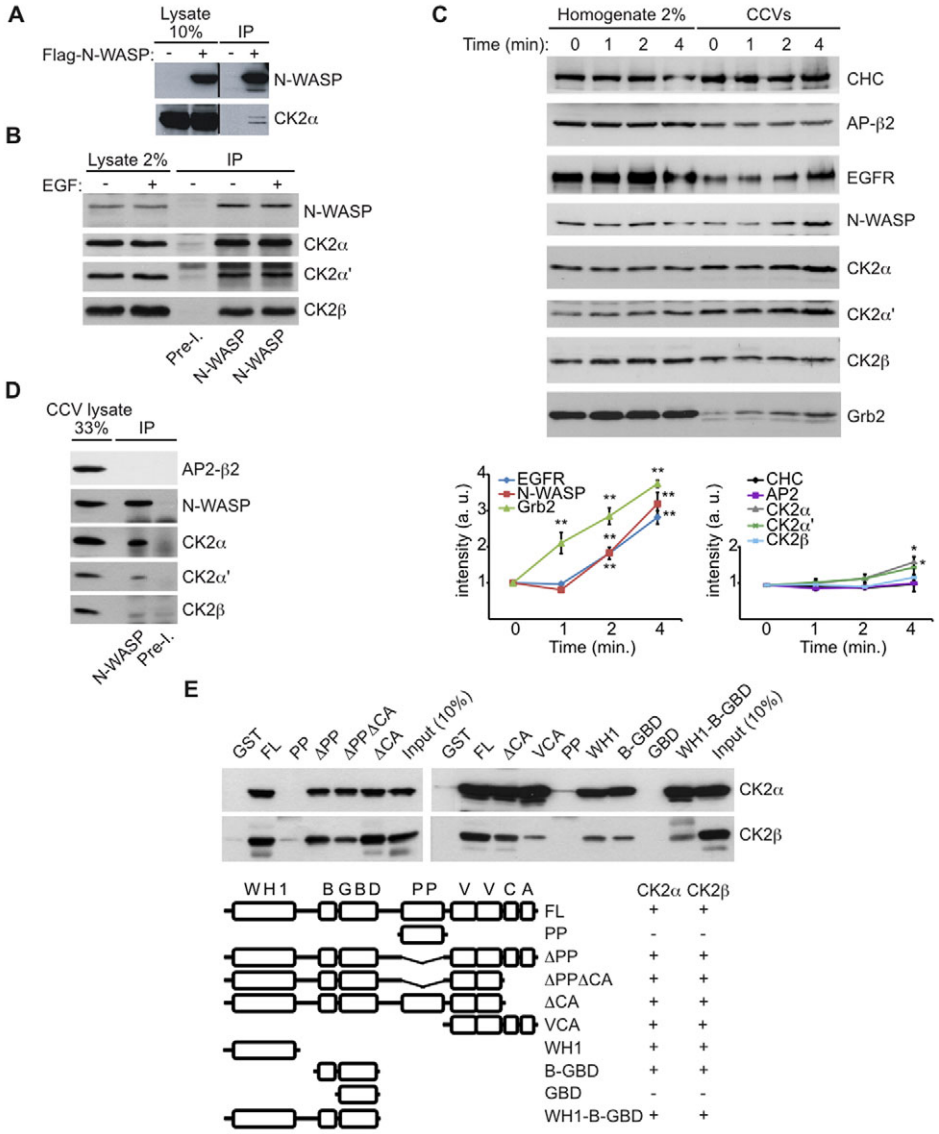

Fig. 1. N-WASP and CK2 form a complex. (**A**,**B**) N-WASP and CK2 coimmunoprecipitate. (A) HEK-293T cells were transfected with Flag-N-WASP (+) or the corresponding empty vector (–). Lysates (1 mg) were incubated with anti-Flag agarose beads. After extensive washes, immunoprecipitates (IP) and lysates (Lysate) were separated by SDS-PAGE and blotted with anti-Flag and anti-CK2α antibodies. One of two experiments that were performed with similar results is shown. (B) HeLa cells were either left untreated (–) or stimulated with EGF (+) (100 ng/ml for 5 minutes). Lysates (1 mg) were incubated with pre-immune rabbit (Pre-I.) or anti-N-WASP anti-serum and Protein-A–agarose beads. Immunoprecipitates were extensively washed, separated on SDS-PAGE and blotted as indicated. One of two experiments that were performed with similar results is shown. (**C**) CCV-recruitment kinetics during CME of the EGFR. The upper panels show cell homogenates and CCVs separated by SDS-PAGE and blotted with the indicated antibodies. The graphs indicate the results of densitometry analysis. Time indicates the duration of EGF stimulation. Results are means±s.d. in all cases (n=3) (**D**) The N-WASP–CK2 complex localizes at CCVs. CCVs were purified from HeLa cells, solubilized and CCV lysates subjected to immunoprecipitation as in B. CCV lysates (33%) and immunoprecipitates were separated by SDS-PAGE and blotted as indicated. One of two experiments that were performed with similar results is shown. (**E**) CK2 binds directly to N-WASP. Recombinant GST-tagged full-length 1 μM rat N-WASP (FL) or deletion mutants thereof (lower-left schematic) were immobilized and incubated with 1 μM soluble purified CK2α (upper panel and lower-right-hand schematic) or CK2β subunit (lower panels and lower-right-hand schematic). Bound proteins were resolved by SDS-PAGE and subjected to immunoblotting as indicated. One of two experiments that were performed with similar results is shown. *0.01<P≤0.05; **0.001<P≤0.01.

To gain insight into the function of the N-WASP–CK2 complex, we analysed the cellular distribution of N-WASP and CK2 and purified CCVs. Bona fide markers of CCVs [clathrin-heavy chain (CHC), adaptor-related protein complex 2 (AP-2) and cyclin-G-associated kinase (GAK), transferrin receptor protein (TfR) and EGFR] proved that CCVs could readily be isolated from HeLa cells. Although they were retrieved mainly in the membrane-containing fractions, N-WASP and CK2 partitioned into both membranes and cytosol (supplementary material Fig. S1C). These results confirm that CK2 is a CCV-associated protein (Bar-Zvi and Branton, 1986; Korolchuk and Banting, 2002) and show that N-WASP localizes on these vesicles. Accordingly, both N-WASP and CK2 partially colocalized with CCSs at the plasma membrane (supplementary material Fig. S2A,B).

CME can be reversibly arrested by incubating cells at restrictive and permissive temperatures, 0°C and 37°C, respectively (Puri et al., 2005). EGF stimulation concomitant with removal of the temperature block triggers a synchronized burst of EGFR internalization (Puri et al., 2005; Sorkin and Goh, 2008). In this way, CCV-associated EGFR functions as a molecular tracer for ligand-induced CME. Rhodamine-conjugated EGF indicated that ligand internalization begins to be clearly detectable at 2 minutes after the release (supplementary material Fig. S2C). Therefore, CCV-enriched fractions were prepared at 1, 2 and 4 minutes after transferring arrested cells to the permissive temperature, with the concomitant EGF stimulation. Cells kept at 0°C remained unengaged in CME and served as a control, whereas EGF-treated cells showed a progressive increase in the amount of EGFR retrieved in the CCV-enriched fraction (Fig. 1C). Grb2 followed the same kinetics as EGFR, as expected from its ability to specifically interact with active EGFR (Jiang et al., 2003). Surprisingly, no major variation in either AP-2 or clathrin was found (Fig. 1C), suggesting that CCV number is either constrained by limiting factors or maintained at the steady state. Alternatively, plasma-membrane-derived CCVs might only constitute a small portion of the total CCVs and, hence, their variation was below our detection limit. Indeed, AP-1 was more efficiently enriched in the CCV-containing fraction than AP-2 (data not shown). Whatever the case, both N-WASP and CK2 subunits could be found in the CCV-enriched fractions and, whereas N-WASP and EGFR displayed similar recruitment kinetics, the amount of CK2 increased less markedly (Fig. 1C).

CK2α and α′ could be specifically detected as proteins co-immunoprecipitating with N-WASP in CCV lysates (Fig. 1D), thus showing that the N-WASP–CK2 complex localizes at CCVs. The low amount of CK2β in the N-WASP immunocomplexes suggested that either holo-CK2, and its isolated subunits, reside in CCVs or holo-CK2 associates with N-WASP by means of α and/or α′ (Fig. 1C).

N-WASP and CK2 interact directly

Immobilized full-length GST–N-WASP and deletion mutants thereof (Fig. 1E, lower-left schematic), or GST as a control, were used to assess whether CK2α and β binding to N-WASP is direct and to map the interaction surfaces. Physical interaction between N-WASP and CK2α could be observed in vitro (Fig. 1E, upper panels). Surprisingly, CK2β bound to N-WASP directly and to the same sites used by CK2α (Fig. 1E, middle and lower panels). The deletion mutants revealed the existence of multiple CK2-interacting surfaces (Fig. 1E), whose availability is likely to be regulated by N-WASP conformation.

CK2 phosphorylates N-WASP both in vitro and in vivo

Serine 480 and 481 of N-WASP are putative acceptor sites for phosphorylation by CK2 (Cory et al., 2003; Meggio and Pinna, 2003) and were mutated to alanine, either singularly or simultaneously. The full-length protein and the VCA domain were purified as GST-fusion proteins to be used in in vitro kinase assays with CK2α. Phosphorylation of wild-type N-WASP and the VCA domain, but not GST alone, indicated that N-WASP is indeed a CK2 substrate (Fig. 2A). The S480A, S481A (hereafter referred to as AA) mutation rendered both N-WASP and its isolated VCA domain resistant to phosphorylation, strongly suggesting that serine 480 and 481 are the only sites targeted by CK2α (Fig. 2A).

Next, we assessed N-WASP phosphorylation both in control and CK2-knockdown (KD) HeLa cells. As a further control for specificity, we took advantage of N-WASP-KD cells. The ablation of N-WASP did not affect the CK2 association with CCVs and vice versa, indicating that independent mechanisms control CK2 and N-WASP localization at CCVs. Phosphorylation of serine 480 and 481 at CCVs was decreased in the absence of CK2 (Fig. 2B). No change was detected in the homogenates, thus suggesting that multiple kinases can phosphorylate N-WASP on the same residues (Fig. 2B). Inhibition of CK2 using 2-dimethylamino-4,5,6,7-tetrabromo-1H-benzimidazole (DMAT) (Pagano et al., 2004) in wild-type cells produced similar effects (supplementary material Fig. S3A). Together, these data highlight the crucial contribution of CK2 to N-WASP phosphorylation at CCVs and also point towards a spatially restricted regulation of N-WASP.

N-WASP is a CK2 inhibitor

Because N-WASP binds to and is phosphorylated by CK2α, it might affect the kinase activity of the latter. CK2α was incubated with a tenfold molar excess of α-casein and GST–N-WASP AA, or α-casein and GST. α-Casein possesses 12 canonical CK2 phosphorylation sites (Meggio and Pinna, 2003) and does not bind to CK2 (data not shown). The phosphorylation-resistant N-WASP was exploited to specifically evaluate the impact of the N-WASP–CK2 interaction on CK2 activity. N-WASP significantly reduced α-casein phosphorylation by CK2 compared with that of the control (Fig. 2C). This inhibitory effect turned out to be primarily exerted by the VCA region (supplementary material Fig. S4A). Furthermore, the incubation of CK2α with a saturating tenfold molar excess of both α-casein and the VCA region strongly diminished the phosphorylation of the former, but not of the latter, compared with that of the controls (Fig. 2D). The phosphorylation-mimicking (S480D and S481D, hereafter referred to as DD) and phosphorylation-resistant mutants of the VCA region were only slightly less effective than the wild-type protein, indicating that the CK2-binding abilities of N-WASP play a key role (Fig. 2D). Most importantly, these experiments collectively suggest that N-WASP can hold CK2 in check by functioning as an inhibitor.

To evaluate the relevance of this phenomenon in a more physiological context, the kinase activity of CCV-associated CK2 was measured on α-casein in control, N-WASP-KD and CK2-KD cells. The kinase activity associated with anti-CK2α antibody immunocomplexes increased in the absence of N-WASP (Fig. 2E,F, supplementary material Fig. S4B). Phosphorylation of α-casein was unambiguously ascribed to CK2, as shown by the lack of phosphorylation in the CK2-KD cells (Fig. 2E). Similar results were obtained assaying intact CCVs (data not shown). In summary, these observations implicate N-WASP in buffering CK2-dependent phosphorylation at CCVs.

Phosphorylation reduces the CK2-binding ability and basal NPF activity of N-WASP

Phosphorylation of serine 480 and 481 by CK2 increases the negative charge at the boundary between the C and A domains in the VCA region. Thus, the affinity of VCA for the B-GBD module might be strengthened (Kim et al., 2000; Prehoda et al., 2000) and N-WASP availability to CK2 reduced. As a result, the affinity of interaction between N-WASP and CK2 should decrease upon phosphorylation. Additionally, phosphorylation might also affect the association of CK2 with the isolated fully available VCA. To

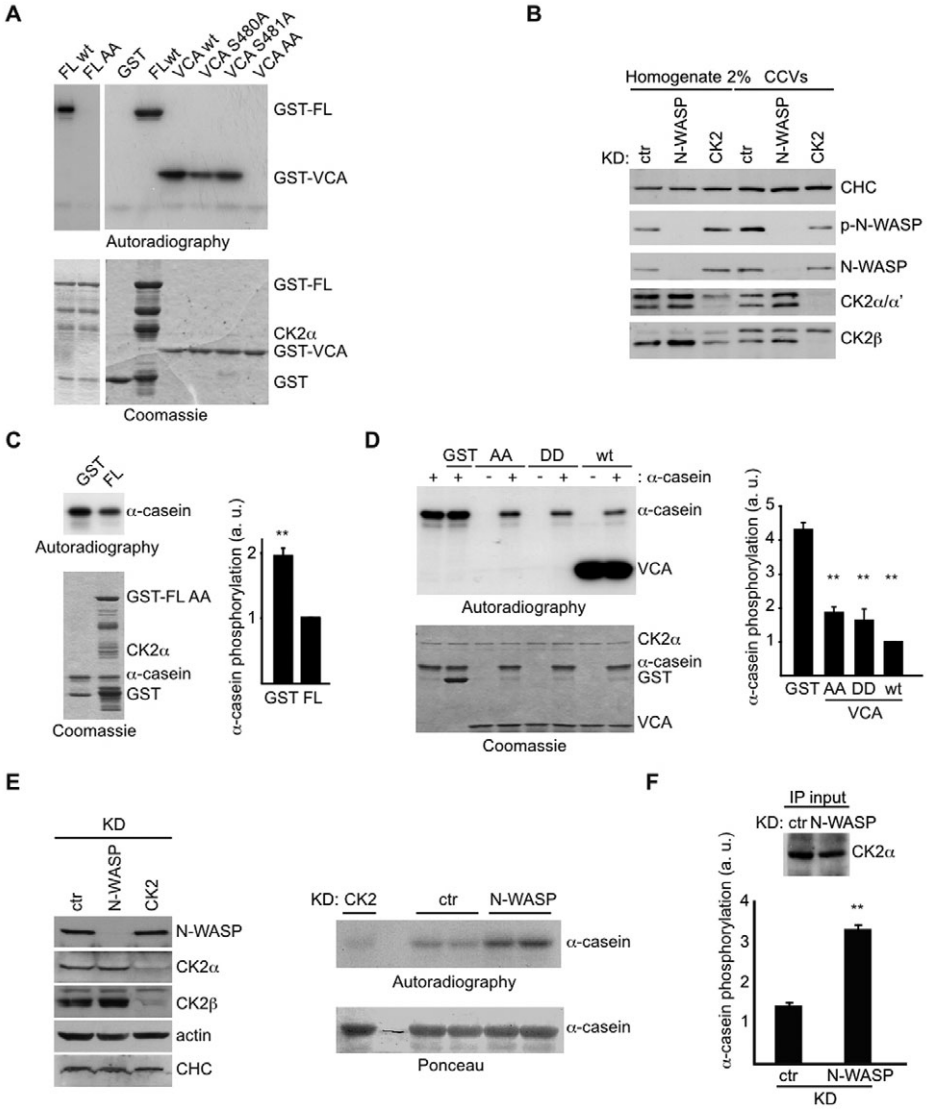

Fig. 2. CK2 phosphorylates and its kinase activity is regulated by N-WASP. (**A**) CK2 phosphorylates N-WASP in vitro. Wild-type GST-tagged full-length N-WASP (FL wt), the S480A and S481A double mutant (FL AA), its isolated wild-type VCA domain (VCA wt) and mutants thereof [VCA S480A, VCA S481A, VCA S480A-S481A (AA)], or GST as a control, were incubated with CK2α as described in the Materials and Methods. Proteins were resolved by SDS-PAGE and the gel stained with Coomassie Brilliant Blue (Coomassie), dried and subjected to autoradiography (Autoradiography). One of two experiments that were performed with similar results is shown. Similar results were obtained with holo-CK2, which simply attained a higher kinase activity towards N-WASP (not shown). (**B**) CK2 phosphorylates N-WASP on CCVs. Homogenates (2%) or solubilized CCVs from control (ctr), N-WASP-KD or CK2-KD (N-WASP and CK2, respectively) cells were analysed by SDS-PAGE and blotted as indicated. One of three experiments that were performed with similar results is shown. Densitometry indicated that N-WASP phosphorylation is reduced to 53±0.1% in CK2 KD cells compared with the control (n=3). The solubility of N-WASP, but not its total expression (see Fig. 4A), reproducibly increases in the absence of CK2. (**C**,**D**) N-WASP inhibits CK2 activity in vitro. (C) Left-hand panel. Kinase assays were performed by incubating 0.2 μM CK2α with 2 μM GST–N-WASP AA or GST along with 2 μM α-casein. Autoradiography and Coomassie-stained gel are illustrated. One experiment of four that were performed with similar results is shown. Right-hand panel. α-casein bands were excised from the gel and the c.p.m. measured. Values were normalized to the lowest value and the relative α-casein phosphorylation plotted. a.u., arbitrary units. (D) Left-hand panel. Kinase assays were performed by incubating 0.4 μM CK2α with 4 μM wild-type VCA (wt), VCA AA (AA), VCA DD (DD), or GST alone, with (+) or without (–) the addition of 4 μM α-casein. One experiment of three that were performed with similar results is shown. Autoradiography and Coomassie-stained gel are illustrated. Right-hand panel. Quantification of three independent experiments was performed as in C and the significance evaluated with one-way ANOVA. (**E**) CK2 displays higher activity on CCVs in the absence of N-WASP. CK2 was immunopurified from CCVs of control (ctr), N-WASP-KD or CK2-KD cells (N-WASP and CK2, respectively) (left-hand panel) and subjected to kinase assays (ctr KD and N-WASP KD were performed in duplicates) using α-casein as a substrate (right-hand panel). One experiment of three that were performed with similar results is shown. (**F**) Quantification of E as in C. **0.001<P≤0.01.

circumvent the inability to achieve complete N-WASP phosphorylation by CK2 in vitro (data not shown), phosphorylation mimetic and resistant mutants were compared. Association equilibrium constants were determined for both GST–N-WASP and GST–VCA with CK2α (supplementary material Fig. S5A–C), the relevant N-WASP-binding partner on CCVs. Although the affinity of the N-WASP AA–CK2α complex was 0.79 μM, that of N-WASP DD and CK2α displayed an 80% reduction (Fig. 3A and supplementary material Fig. S5D,E). By contrast, the interaction affinities of CK2α with GST–VCA AA and DD were indistinguishable (0.133 compared with 0.137 μM) (Fig. 3A; supplementary material Fig. S5F,G), ruling out that extra negative charges result in VCA interacting less efficiently with CK2α. In keeping with the above results, non-saturating concentrations of N-WASP DD activated the Arp2/3 complex less efficiently than N-WASP AA (Fig. 3B and supplementary material Fig. S6A,B). Cdc42-dependent activation showed that the two mutants attained similar maximal activities (supplementary material Fig. S6B). Consistently, the NPF activities of VCA AA and DD could not be distinguished (Fig. 3D).

CK2 binding decreases the NPF activity of N-WASP

To investigate whether activation of the Arp2/3 complex by N-WASP is sensitive to CK2 binding, a saturating concentration of CK2α was added to either full-length N-WASP or its isolated VCA domain. Both wild-type and kinase-dead (K68A) CK2α, as well as holo-CK2, strongly inhibited the NPF activity of N-WASP (Fig. 3B,C). By contrast, the constitutively active VCA domains were only marginally affected (Fig. 3D). CK2α did not alter actin polymerization on its own (Fig. 3C), nor did it phosphorylate or bind to the Arp2/3 complex (supplementary material Fig. S6C,D), thus ruling out N-WASP-independent effects. CK2β did not modulate the activity of N-WASP, demonstrating the specificity of CK2α in regulating N-WASP (Fig. 3C). Notably, GTPγS-bound Cdc42 relieved N-WASP inhibition by CK2α (Fig. 3E). Hence, binding of CK2 to N-WASP results in VCA inhibition through a mechanism that might stabilize the closed conformation of N-WASP. CK2 deploys two mechanisms (i.e. phosphorylation and binding) to regulate N-WASP activity and can be considered as the founding member of a new class of N-WASP inhibitors.

A

	FL AA	FL DD	VCA AA	VCA DD
K_D (μM)	0.786	4.109	0.137	0.133
SD (μM)	0.12	0.88	0.0038	0.0043

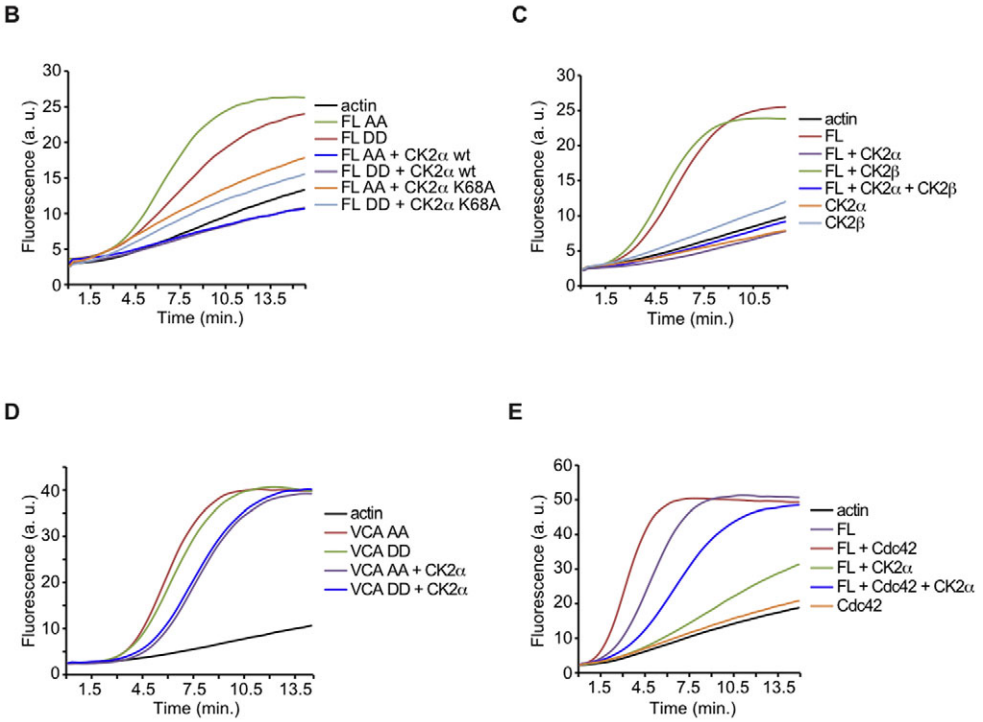

Fig. 3. CK2 regulates N-WASP. (**A**) N-WASP AA displays higher affinity for CK2α than DD. Surface plasmon resonance measurements of the interactions between CK2α and the indicated N-WASP mutants were performed to derive equilibrium dissociation constants (means±s.d.; $0.001<P\leq0.01$ for FL AA compared with FL DD; $n=5$). Sensograms are presented in supplementary material Fig. S5D–G. (**B**) NPF activity of N-WASP AA and N-WASP DD and effects of CK2α. Pyrene-actin polymerization assays were performed with 15 nM GST–N-WASP (either AA or DD) and 1 μM wild-type (wt) or kinase-dead (K68A) CK2α. (**C**) CK2α and holo-CK2, but not CK2β, inhibit N-WASP. N-WASP AA was assayed, as in B, with 1 μM CK2α and 1 μM CK2β. CK2β slightly stimulated actin polymerization in the absence of N-WASP, whereas holo-CK2 did not (not shown). Identical results were obtained with N-WASP DD (not shown). (**D**) NPF activity of VCA AA and VCA DD and effects of CK2α. 1 μM CK2α and 250 nM GST-VCA AA or DD were used. Identical results were obtained with wild-type GST–VCA (not shown). (**E**) Cdc42 relieves N-WASP inhibition by CK2α. Conditions were as in C, but with 1 μM GTPγS-loaded Cdc42 (Cdc42).

N-WASP and CK2 jointly regulate clathrin-mediated endocytosis and cell-surface levels of the EGFR

Stable N-WASP-KD HeLa cells could be readily generated (Fig. 4A), whereas transient co-silencing of either CK2α and α′ or all three CK2 subunits was required to strongly reduce of CK2 expression (data not shown; Fig. 4A). Importantly, downregulation of CK2 and N-WASP, either alone or in combination, did not affect the expression levels of EGFR or the Arp2/3 complex (Fig. 4A). Low doses of iodinated EGF were used to selectively induce EGFR endocytosis through the clathrin-dependent pathway and to measure its initial rate of internalization (Sigismund et al., 2005). The removal of N-WASP resulted in a decreased EGF internalization rate compared with that in control cells (Fig. 4B). CK2-KD cells showed a similar phenotype and the concomitant silencing of N-WASP and CK2 did not further reduce the internalization rate (Fig. 4B). Knockdown of the Arp2/3 complex phenocopied the absence of the N-WASP–CK2 complex. These results suggest that CK2 and N-WASP act together in a pathway, with the Arp2/3 complex as the end-effector, to modulate CME of EGFR.

Notably, downregulation of either N-WASP or CK2 increased the cell-surface levels of EGFR without affecting its expression and recycling (Fig. 4A–C and supplementary material Fig. S7, respectively). The observation that knockdown of both N-WASP and CK2 failed to induce either additive or synergistic effects, compared with the single knockdowns, further supports that N-WASP and CK2 represent a functional unit (Fig. 4B–D). Taken together, these data indicate that N-WASP and CK2 jointly optimize CME of the EGFR.

N-WASP and CK2 activities and their ability to enter into a complex control cell-surface levels of EGFR

To assess the physiological relevance of N-WASP phosphorylation, we transfected N-WASP-KD cells with short hairpin RNA (shRNA)-insensitive EGFP-tagged wild-type, phosphorylation-resistant or phosphorylation-mimicking N-WASP and analysed cell-surface EGFR. Total EGFR was not affected by reintroducing either wild-type N-WASP or its phosphorylation mutants (data not shown). However, wild-type N-WASP reduced the amount of EGFR at the plasma membrane (Fig. 5A,B). Although the effect of N-WASP DD was indistinguishable from that of the wild type, EGFP alone and N-WASP AA did not cause a significant decrease in plasma membrane EGFR (Fig. 5A,B). The identical maximal

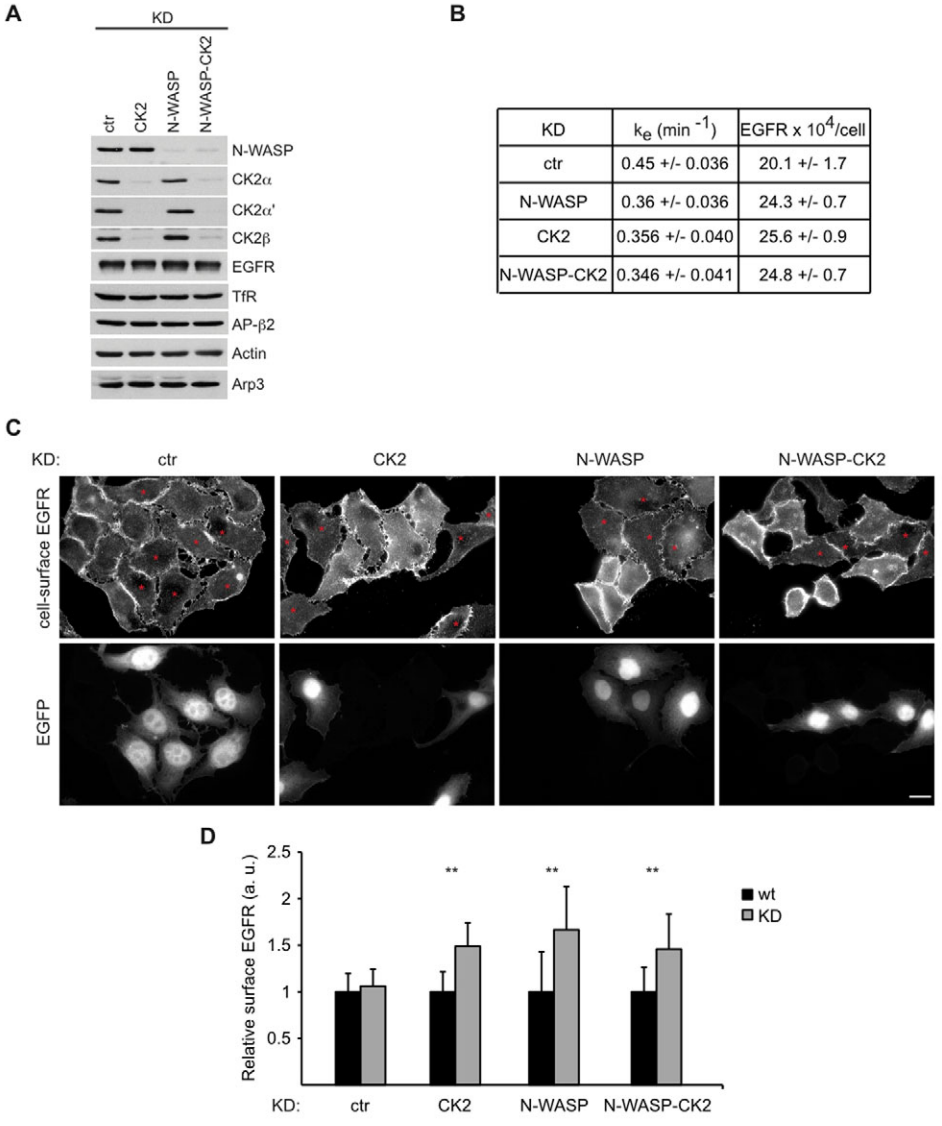

KD	k_e (min $^{-1}$)	EGFR x 10^4/cell
ctr	0.45 +/- 0.036	20.1 +/- 1.7
N-WASP	0.36 +/- 0.036	24.3 +/- 0.7
CK2	0.356 +/- 0.040	25.6 +/- 0.9
N-WASP-CK2	0.346 +/- 0.041	24.8 +/- 0.7

Fig. 4. N-WASP-KD and CK2-KD cells display decreased EGF endocytosis. (**A**) Characterization of HeLa knockdown cells. Representative immunoblot analysis of relevant proteins (indicated on the right) in the various knockdown (KD) cells (indicated on top). Equal amounts of total cellular lysates were used; TfR and actin served as loading controls. (**B**) Initial rate of EGF internalization (k_e; minute^{-1}) [means±s.d.; $0.01<P\leq0.05$ for all KDs compared with the control KD (ctr); $n=9$] and the number of EGFRs on the plasma membrane (means±s.d.; $0.01<P\leq0.05$ for all KDs compared with the ctr; $n=6$) in N-WASP-KD (N-WASP), CK2-KD (CK2) and in N-WASP and CK2 double-knockdown (N-WASP-CK2) cells. (**C**) Removal of N-WASP and CK2 increases EGFR at the cell surface. Control HeLa cells, stably expressing EGFP, were mixed with the indicated KD cells, seeded on coverslips and then left in 0.1% fetal calf serum. The next day cells were fixed and cell-surface EGFR was selectively marked. Representative wide-field pictures are shown. EGFP-positive cells are marked with a red asterisk in the cell-surface EGFR panels. Scale bar: 20 µm. (**D**) N-WASP-KD, CK2-KD and N-WASP and CK2 double-knockdown cells are phenocopies. Surface EGFR intensities displayed by knockdown and neighbouring EGFP-positive wild-type cells were measured and plotted for each mixed population. Data are means+s.d. for four independent experiments performed as in C. One-way ANOVA was used to assess statistical significance. $**0.001<P\leq0.01$.

NPF activities of these two N-WASP mutants (supplementary material Fig. S6B) suggest that proper CK2-binding abilities are also crucial for N-WASP function. Indeed, the phosphorylation-mimicking mutant bound to CK2α more efficiently with respect to its phosphorylation-resistant counterpart (Fig. 5C). These findings agree with phosphorylation of serine 480 and 481 being required for N-WASP to accumulate on CCVs upon EGF stimulation (supplementary material Fig. S1G and not shown) and highlight

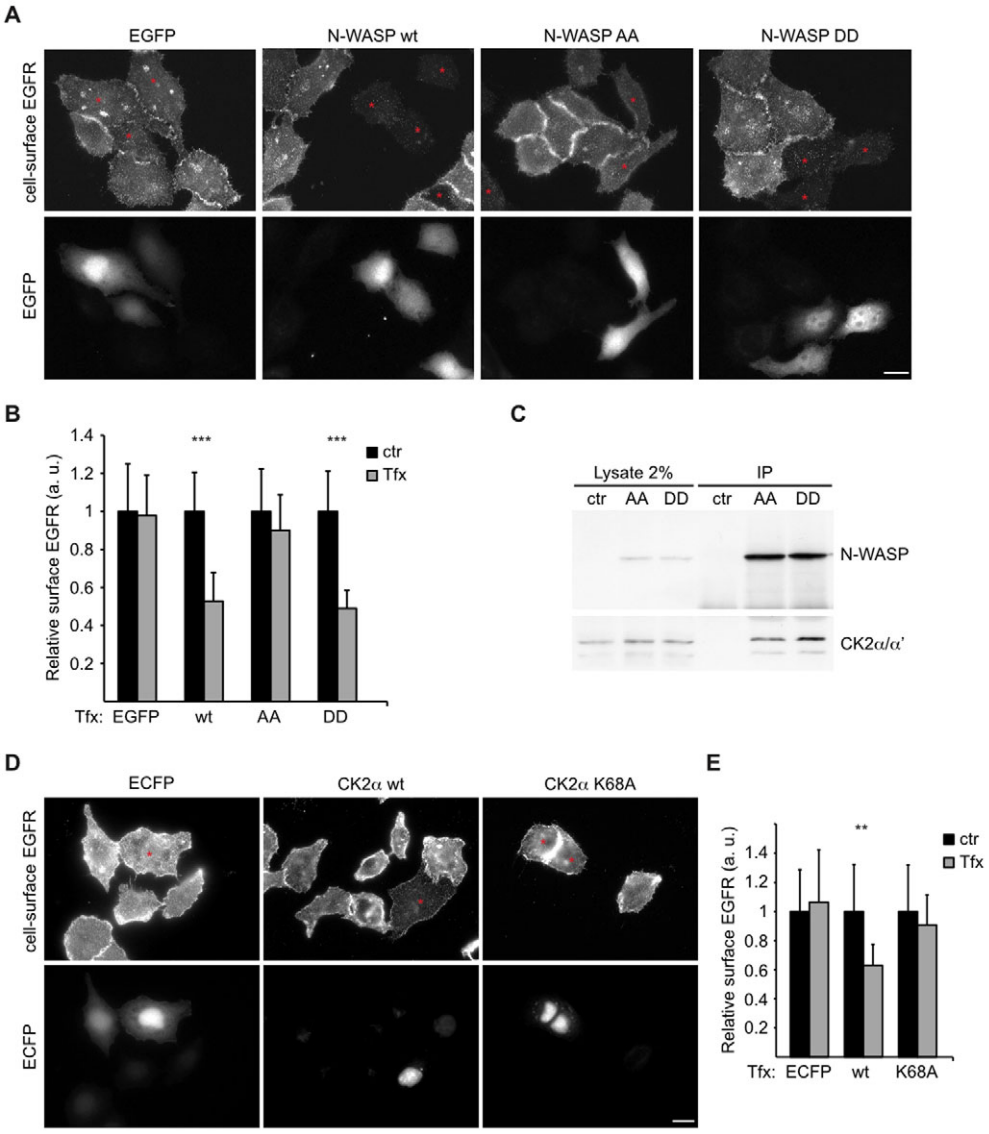

Fig. 5. Wild-type and phosphorylation-mimicking N-WASP and wild-type CK2α efficiently rescue cell-surface EGFR levels. (**A**) Wild-type and phosphorylation-mimicking, but not phosphorylation-resistant, N-WASP affect cell-surface EGFR levels in N-WASP-KD cells. N-WASP-KD cells were transfected with shRNA-insensitive wild-type EGFP–N-WASP (N-WASP wt), its phosphorylation-resistant (N-WASP AA) and phosphorylation-mimicking (N-WASP DD) mutants, or the empty vector (EGFP). Cells were left in 0.1% fetal calf serum, fixed and stained as in Fig. 4C. Representative wide-field pictures are shown. All transfectants are marked with a red asterisk in the cell-surface EGFR panels. Scale bar: 20 µm. shRNA-insensitive EGFP–N-WASPs were expressed at similar levels in N-WASP KD cells (not shown). (**B**) N-WASP wild type and DD decrease cell-surface EGFR in N-WASP-KD cells. Surface EGFR was determined as described in the Materials and Methods. Data are means±s.d. for five independent experiments performed as in A. ctr, control; Tfx, transfected; wt, N-WASP wild type; AA, N-WASP AA; DD, N-WASP DD. One-way ANOVA was used to assess statistical significance. ***$P \leq 0.001$. (**C**) Correlation between the rescuing abilities of N-WASP AA and DD and their binding to CK2. N-WASP-KD cells were transfected with shRNA-insensitive EGFP–N-WASPs (either AA or DD), or were mock-treated (ctr). Immunoprecipitations (IP) with the anti-N-WASP serum were performed as in Fig. 1B, separated on SDS-PAGE and blotted as indicated. The CK2:N-WASP ratio was calculated for both the AA and DD lanes as in supplementary material Fig. S1H and values were normalized with respect to DD. The amount of CK2α and α′ co-immunoprecipitating with N-WASP AA is reduced to 54±4% compared with that of N-WASP DD. Similar results were obtained by expressing GST–N-WASP AA and DD in HEK-293T cells (not shown). (**D**) Wild-type, but not kinase-dead, CK2α affects cell-surface EGFR levels upon knockdown of both CK2α and α′. siRNA-insensitive ECFP-tagged wild-type (CK2α wt) and kinase-dead (CK2α K68A) CK2α, or ECFP alone, were transfected in CK2α and CK2α′ double-knockdown cells. Cells were fixed and stained for surface EGFR as in A. Representative wide-field pictures are shown. All transfectants are marked with a red asterisk in the cell-surface EGFR panels. Scale bar: 20 µm. The cells expressing wild-type CK2α were typically two times more abundant than CK2α K68A transfectants in the CK2α and CK2α′ double-knockdown cells (not shown). (**E**) Wild-type CK2α decreases cell-surface EGFR in CK2α and α′ double-knockdown KD cells. Quantification was performed as in B. Data are means±s.d. for three independent experiments performed as in D. wt, CK2α wt; K68A, CK2α K68A.

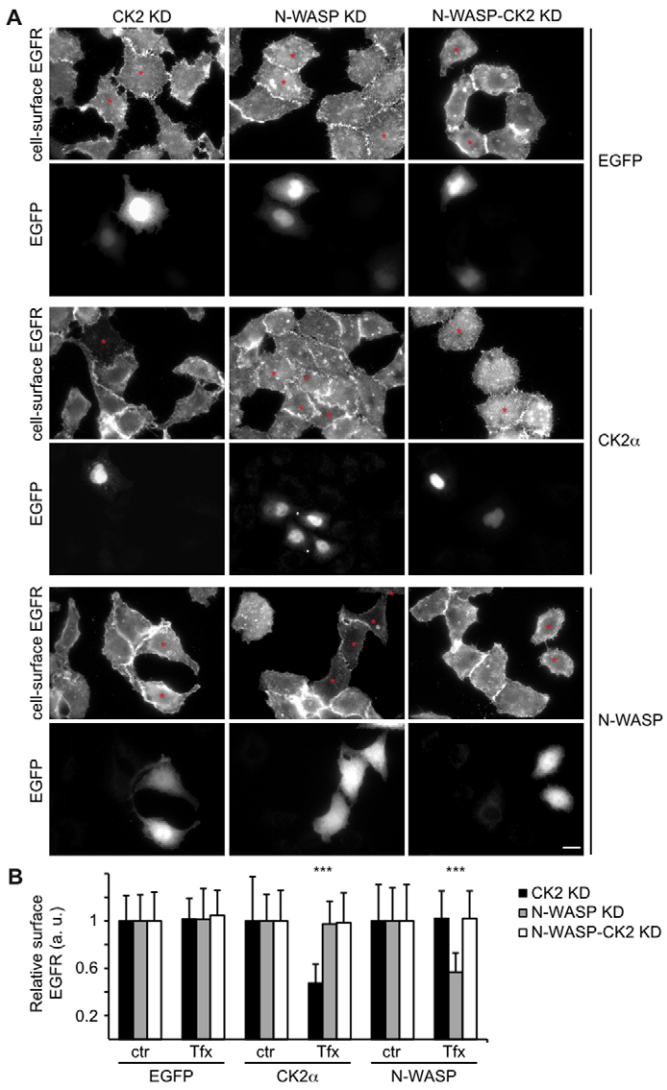

Fig. 6. Cell-surface EGFR levels can only be rescued by reconstituting the N-WASP-CK2 complex. (**A**) Cell-surface EGFR levels in CK2α and CK2α′ double-knockdown (CK2), N-WASP-KD and N-WASP, CK2α and CK2α′ triple-knockdown (N-WASP-CK2) cells transfected with EGFP, EGFP–CK2α or EGFP–N-WASP. Knockdown cells were transfected with shRNA-insensitive wild-type EGFP–N-WASP, siRNA-insensitive wild-type EGFP–CK2α, or EGFP alone. Cells were left in 0.1% fetal calf serum, fixed and stained as in Fig. 4C. Representative wide-field pictures are shown. All transfectants are marked with a red asterisk in the cell-surface EGFR panels. Scale bar: 20 µm. (**B**) The simultaneous presence of CK2 and N-WASP is required for controlling cell-surface EGFR levels. Data are means±s.d. for three independent experiments performed as in A and quantified as in Fig. 5B. ctr, control; Tfx, transfected. One-way ANOVA was used to assess statistical significance. ***$P \leq 0.001$.

that the CK2-binding and CME-rescuing abilities of N-WASP are correlated.

We also reconstituted CK2α and CK2α′ double-knockdown cells with either RNA interference (RNAi)-insensitive wild-type or kinase-dead (K68A) CK2α, or ECFP alone as a control. A significant reduction in cell-surface EGFR could be detected in ECFP–CK2α-expressing cells (Fig. 5D,E). By contrast, CK2α K68A did not reduce the levels of cell-surface EGFR (Fig. 5D,E), thus indicating that the kinase activity is essential for this CK2 function. The rescue was not due to a change in total EGFR (data not shown). Most importantly, the rescuing effect of CK2 requires N-WASP because ectopic expression of CK2α failed to decrease surface levels of EGFR when CK2α, CK2α′ and N-WASP were all simultaneously knocked down (Fig. 6); the same holds true for N-WASP (Fig. 6). In summary, the ability of N-WASP and CK2 to properly regulate CME of the EGFR correlates with their proficiency to assemble in a complex and requires their activities.

N-WASP and CK2 regulate F-actin at CCSs

Our observations predict that the perturbation of the function of the N-WASP–CK2 complex should alter actin dynamics at forming CCPs. Therefore, control, N-WASP-KD and CK2-KD cells, as well as N-WASP and CK2 double-knockdown cells, were analysed for F-actin association with CCSs through total internal reflection (TIRF) microscopy. In control cells, phalloidin-labelled actin could be detected in ~70% of peripheral CCSs (Fig. 7A,B). Strikingly, most CCSs were devoid of F-actin in both N-WASP and the N-WASP and CK2 double knockdowns (Fig. 7A,B). Thus, N-WASP appears to be central for the presence of F-actin at CCSs. Although the absence of CK2 did not affect the percentage of F-actin-positive CCSs (Fig. 7A,B), its pharmacological inhibition (Pagano et al., 2004) resulted in a 25% reduction in the internalization rate constant (k_e) of the EGFR, in more CCSs being F-actin-free (supplementary material Fig. S3B–D) and in less N-WASP accumulating on CCVs upon EGF stimulation in wild-type HeLa cells (supplementary material Fig. S1G). The finding that DMAT treatment phenocopies N-WASP but not CK2 silencing agrees with the notion of N-WASP inactivation upon CK2 binding and suggests that affinity-regulated assembly of the N-WASP–CK2 complex is crucial for actin polymerization at CCPs. The robust association between F-actin and CCPs is surprising given that actin recruitment is often only transient (Benesch et al., 2005; Ferguson et al., 2009; Innocenti et al., 2005; Lamaze et al., 1997; Merrifield et al., 2005; Merrifield et al., 2004; Yarar et al., 2005). However, the large cytosolic free pool and detrimental effects of mRFP and EGFP-tagged G-actin on actin dynamics (Riedl et al., 2008) might have resulted in an underestimation of the colocalization between F-actin and CCPs.

Discussion

The present study describes the first example of concerted action by kinases and actin during CME in mammalian cells. In this context, the N-WASP–CK2 complex represents a molecular platform that integrates different elements contributing to EGFR internalization in a single circuit. Notably, both N-WASP and CK2 activities and their abilities to assemble in a complex are required for the proper execution of this process.

We have shown that N-WASP fulfils both NPF-dependent and NPF-independent roles in CME: it promotes actin polymerization by the Arp2/3 complex and inhibits CK2, respectively. Both functions depend upon the CK2-binding abilities of N-WASP, which are regulated by phosphorylation. Upon phosphorylation of serine 480 and 481, N-WASP shows decreased CK2-binding and Arp2/3-complex-activating abilities. We did not record differences between phosphorylation-mimicking and phosphorylation-resistant N-WASP after Cdc42-mediated derepression (supplementary material Fig. S6B). At odds with this, WASP can be converted into a more potent NPF by CK2 phosphorylation (Cory et al., 2003). Technical aspects, including the use of Cdc42-insensitive WASP, along with structural differences between WASP and N-WASP might account for these discrepancies.

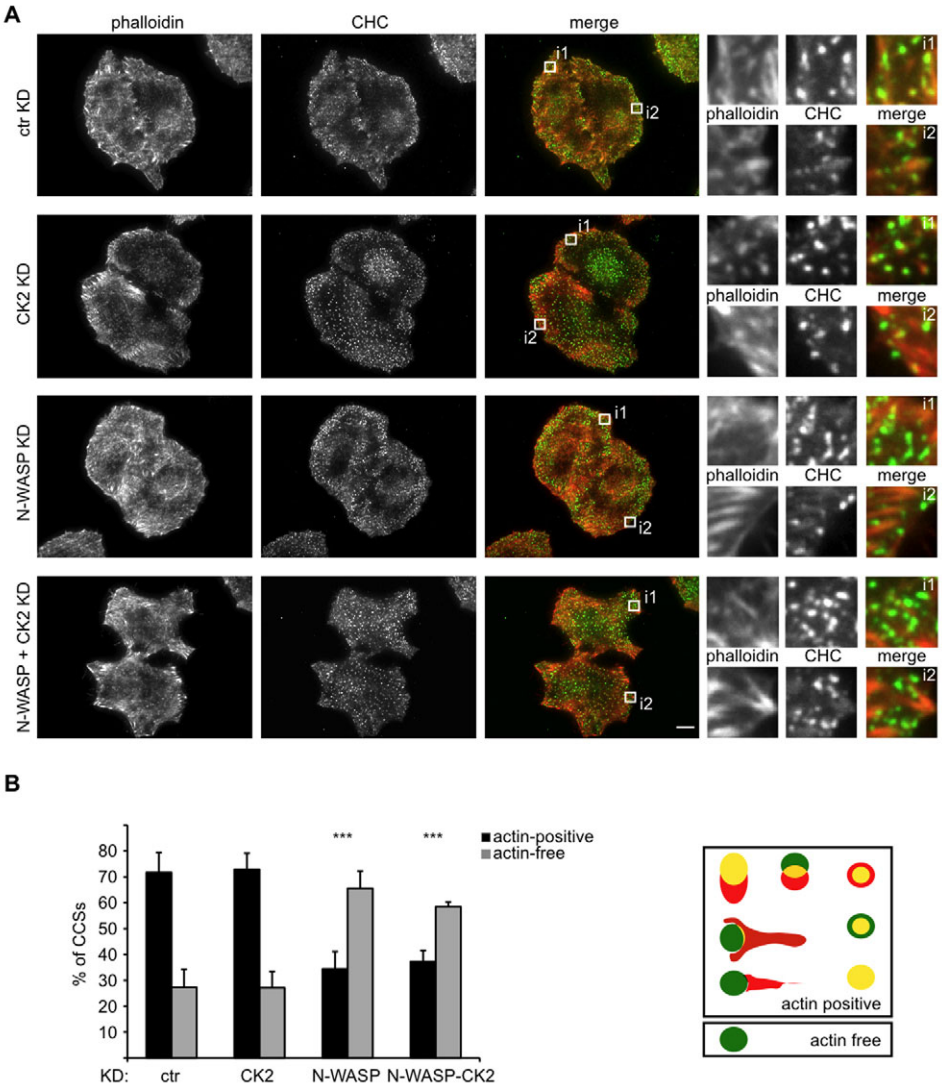

Fig. 7. N-WASP and CK2 regulate actin dynamics at clathrin-coated structures. (**A**) Morphology and association of F-actin with CCSs in control KD, CK2-KD, N-WASP-KD and N-WASP and CK2 double-knockdown cells. Knockdown cells were fixed and stained with anti-clathrin heavy chain (CHC, green in the 'merge' image) antibodies and rhodamine–phalloidin (phalloidin, red in the merge) to detect CCSs and F-actin, respectively. Representative TIRF micrographs are illustrated. Enlarged images are shown on the right. Scale bar: 10 µm. (**B**) N-WASP controls the presence of F-actin at CCSs. Left-hand panel. Quantification was performed as explained in the Materials and Methods. Data are means±s.d. for two independent experiments as in A, in which at least five pictures per condition and 50 CCSs per cell were inspected. Two-way ANOVA was used to assess statistical significance. ***$P \leq 0.001$. Right-hand panel. Schematic of the scored phenotypes and their classification. CHC, green; actin, red; yellow, colocalization of CHC and actin.

We also demonstrated that CK2 is required for optimal clathrin-dependent internalization of the EGFR. To fulfil this function, CK2 modulates the actin-regulatory machinery involved in CME by means of both its scaffolding and kinase activities. Several lines of evidence support this interpretation. First, kinase-dead CK2α failed to rescue the increased cell-surface EGFR levels in CK2-KD cells. Second, both silencing and pharmacological inhibition of CK2 impaired EGFR internalization, despite having opposite effects on N-WASP activity. Nevertheless, the N-WASP and CK2 double-knockdown cells did not reveal either additive or synergic effects with respect to the single knockdowns, nor did DMAT further decrease the initial rate of endocytosis of EGF in N-WASP-KD cells (data not shown). Thus, phosphorylation-mediated regulation by CK2 probably extends to additional targets contributing to N-WASP-promoted actin dynamics at CCPs. Interestingly, several components of the actin machinery and N-WASP-binding proteins are potential CK2 substrates (Meggio and Pinna, 2003). Third, and in contrast to a previous report (Korolchuk and Banting, 2002), we found that CK2 is active in the intact CCV-enriched fraction (data not shown). Fourth, the scaffolding abilities and kinase activity of CK2 are crucial for N-WASP inhibition.

Interplay between N-WASP and CK2 is based on assembly of the N-WASP–CK2 complex. The cellular concentrations of N-WASP and CK2 (0.33 and 0.66 µM, respectively), their membrane-associated fractions (70% and 50% of the total, respectively) and high N-WASP phosphorylation at the steady state (~90%) (supplementary material Fig. S1D–F), indicate that a membrane-bound N-WASP–CK2 complex can exist only where both partners are sufficiently concentrated and impose spatial constraints to its formation. The EGF-induced accumulation of N-WASP on CCVs sets conditions favourable to the localized assembly of the N-WASP–CK2 complex and causes CK2 to become limiting on nascent CCVs (supplementary material Fig. S1G,H). As a result, the CCP-associated free fraction of N-WASP is able to boost actin polymerization when CK2 activity is minimal. Hence, the N-WASP–CK2 complex has the potential to initiate and to terminate the action of N-WASP and CK2, respectively. This solves the paradox of the positive role played by the N-WASP–CK2 complex despite it having reduced NPF and kinase activities. We propose that CCP maturation is accompanied by an increase in N-WASP-dependent actin polymerization and a progressive reduction in CK2 activity orchestrated by the N-WASP–CK2 complex (Fig. 8).

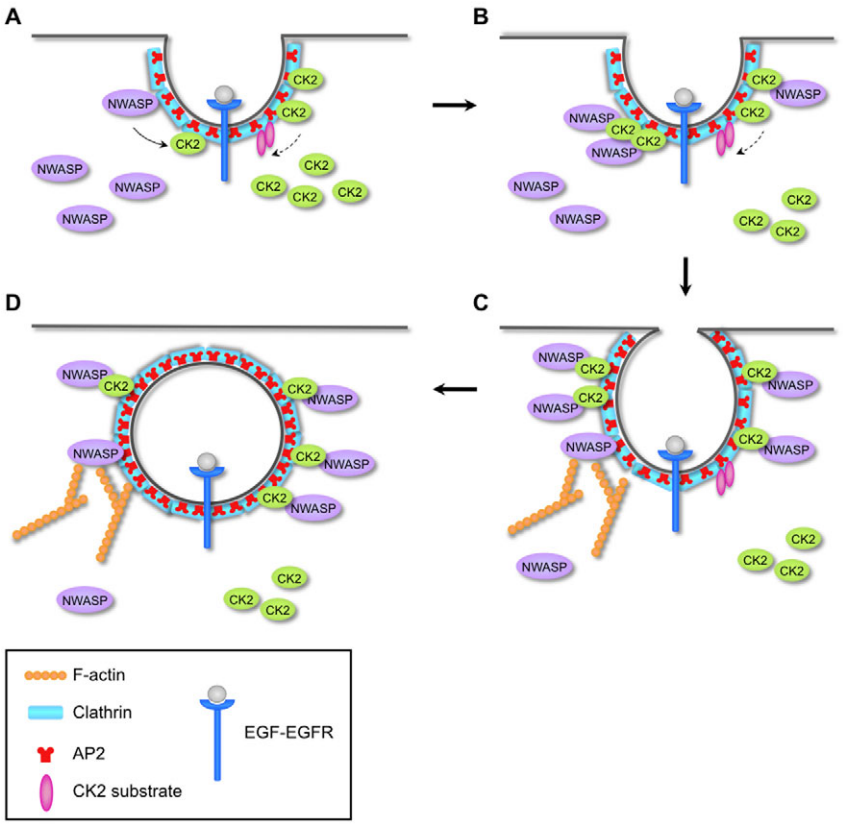

Fig. 8. Proposed mechanism regulating the contribution of the N-WASP–CK2 complex to CME. (**A**) CCPs loaded with activated EGFR recruit N-WASP and CK2 by means of two independent pathways. This results in the assembly of the N-WASP–CK2 complex (indicated by a solid arrow). The N-WASP–CK2 complex has reduced NPF and kinase activities compared with that of its isolated subunits. Initially, there is more CK2 than N-WASP bound to CCPs. CCP-associated CK2 is able to phosphorylate (dashed arrow) unknown proteins (pink ovals) involved in actin dynamics at CCPs and/or CCVs. In addition, phosphorylated N-WASP might be more efficiently retained on CCPs. (**B**) Although N-WASP accumulates on maturing CCPs with time, levels of CK2 remain substantially unchanged. Draining the CCP-associated free pool of CK2 progressively reduces the ability of CK2 to phosphorylate its targets. (**C**) At the late stages of CCV biogenesis, all CCP-associated CK2 is trapped in the N-WASP–CK2 complex and its kinase activity reaches a minimum. The CCP-associated free fraction of N-WASP promotes Arp2/3-complex-dependent actin polymerization. (**D**) N-WASP binding to CCPs peaks just prior to fission, thus boosting the formation of new actin filaments that contribute to pinching off a CCV.

Consequently, the N-WASP–CK2 complex controls the contribution of its subunits to CME of EGFR. The integration of kinase and actin functions in a single circuit reveals a new pathway that sheds more light on our mechanistic view of CME.

Materials and Methods

Vectors, antibodies and reagents

pECFP-CK2α and pGEX-3-CK2β were gifts from Ellen Haugsten (Institute for Cancer Research, The Norwegian Radium Hospital, Oslo, Norway). pGEX-4T-3-CK2α, pGEX-4T-3-CK2α K68A and pECFP-CK2α were subcloned from pSG5-CK2α and pSG5-CK2α-HA, which were gifts from Yves Goldberg (Commissariat a l'Energie Atomique, Grenoble, France). Full-length rat N-WASP (amino acids 1–501), ΔCA (amino acids 1–446), VCA (amino acids 394–501), PP (amino acids 274–400), WH1 (amino acids 1–182), B-GBD (amino acids 183–273), GBD (amino acids 200–273), WH1-GBD (amino acids 1–273) were amplified by PCR and cloned into pGEX-6P-1 vector. pCDNA3 Flag-N-WASP (2–501) was obtained by PCR. Rat N-WASP S480A, S481A (AA), N-WASP S480D, S481D (DD), shRNA-insensitive N-WASP and RNAi-insensitive CK2α were generated by site-directed mutagenesis (Stratagene). pRK-GST-N-WASP (wild type, AA and DD) were obtained by subcloning. All constructs were verified by sequencing.

Goat anti-CK2α antibody, goat anti-CK2α′ antibody, rabbit anti-CK2β antibody, rabbit anti-GAK antibody, goat anti-clathrin-heavy-chain antibody, mouse anti-GST antibody, goat anti-Arp3 antibody and mouse anti-CD71 antibody (against the transferrin receptor) were from Santa Cruz Biotechnology. Mouse anti-CK2α and α′ antibody was from BD Biosciences, and mouse anti-clathrin-heavy-chain antibody was from ABR. Mouse anti-EGFR antibody (Ab-1) was from Oncogene. Mouse anti-AP-2 antibody (β2) and mouse anti-p21-ARPC3 antibody were from Transduction Laboratories. Mouse anti-Flag antibodies and mouse anti-actin antibody were from Sigma. Rabbit monoclonal anti-N-WASP antibody was from Cell Signaling. Mouse anti-clathrin-heavy-chain antibody (X-22) was from ABR. Polyclonal rabbit anti-N-WASP antibodies were generated against full-length GST–N-WASP according to standard procedures. Antibodies against N-WASP-*P* (phosphorylated serines 480 and 481) were from UBL. Rabbit-anti Sec22 antibody was a gift from Tiziana Scanu (The Netherlands Cancer Institute, Amsterdam, The Netherlands). Alexa-Fluor-488- or Alexa-Fluor-555-conjugated secondary antibodies and DAPI were from Invitrogen. If not otherwise specified, all chemicals were from Sigma.

Biochemical assays

Standard procedures for protein analysis, in vitro binding, protein purification, cell lysis and immunoprecipitation were as previously described (Beli et al., 2008; Innocenti et al., 2004). Full-length N-WASPs used in all actin polymerization assays and Biacore experiments were purified from mammalian cells in a manner similar to that previously described for WAVE2 (Innocenti et al., 2004). Anti-GST antibodies were used to confirm correct loading in all pull-down experiments (data not shown). Cleavage of full-length CK2α and CK2β from GST was performed with thrombin (Novagen) and Factor Xa (Amersham Biosciences), respectively. Cleavage of VCAs from GST was performed with the Pre-scission protease (GE Healthcare).

Surface plasmon resonance

The Biacore X100 system was used. Goat anti-GST antibodies were covalently linked to Sensor Chip CM5 (Biacore), with the amine-coupling and GST-capture kits (Biacore), according to the manufacturer's instructions. Approximately 200 relative units (RU) of recombinant GST–N-WASP AA or DD were captured onto the chips. CK2α was diluted in HBS-EP running buffer [0.01 M HEPES pH 7.4, 0.15 M NaCl, 3 mM EDTA and 0.005% (v/v) Surfactant P20] and injected with a flow rate of 15 μl per minute. Multi-cycle kinetics was performed. The surface was regenerated with 10 mM glycine-HCl pH 2.2 according to the GST capture kit instructions. The response in the control flow cell, which had a comparable amount of GST captured onto the surface, was subtracted from each sensogram. Data were analysed with Biacore Evaluation Software according to a 1:1 binding model.

Kinase assays

Purified recombinant GST-fusion proteins, attached to glutathione–Sepharose 4B beads, soluble CK2α and/or CK2β, or immunoprecipitates bound to Protein A beads, were resuspended in 30 μl kinase buffer (50 mM Tris-HCl pH 7.4, 150 mM NaCl, 10 mM $MgCl_2$ and 20 μM ATP), supplemented with 2.5 μCi [γ-^{32}P]ATP (Invitrogen) and incubated at 30°C for 20 minutes. Reactions were boiled in sample buffer and resolved by SDS-PAGE, then either stained with Coomassie Brilliant Blue, dried and subjected to autoradiography or transferred onto nitrocellulose membrane, subjected to autoradiography and subsequent western blotting.

Generation of knockdown cells

N-WASP-KD cells were created by infecting wild-type HeLa cells with pRS-N-WASP (target sequence: 5′-GGAGCAAAGCCATTCATTC-3′), followed by selection with puromycin (2.5 μg/ml) and clone isolation. Three selected single clones were further characterized for N-WASP protein levels and the response to EGF. Because similar results were obtained, all the subsequent experiments were then performed with only

one clone. Oligofectamine (Invitrogen) was exploited to deliver siRNA duplexes into cells. CK2α-KD cells were obtained with the target sequence 5′-CAAGATGACT-ACCAGCTGG-3′ (Dharmacon); CK2α′- and CK2β-KD cells were obtained with siGENOME SMARTpool human CSNK2A2 and CSNK2B (Dharmacon), respectively. Initially, parallel sets of cells were transfected with siCONTROL non-targeting siRNA (Dharmacon) or were mock-transfected to provide essential controls. No differences could be found and thereafter only the latter was performed. In all cases, cells were transfected twice according to Dharmacon's instructions and analysed 3 days after the first round of transfection, as previously described (Beli et al., 2008). p21-ARPC3-Arp3-KD cells were obtained, as previously described (Beli et al., 2008).

Clathrin-coated vesicle purification

After overnight starvation in Dulbecco's modified Eagle's medium (DMEM) containing 0.1% serum, either 15×10^6 (Fig. 1C, supplementary material Fig. S1C,G,H and supplementary material Fig. S4B) or 5×10^6 HeLa cells (Fig. 2E,F) were supplemented with 50 mM HEPES pH 7.4 and incubated on ice for 1 hour. To release the temperature block and concomitantly induce EGFR internalization, this medium was replaced by pre-warmed medium supplemented with EGF (100 ng/ml) and cells were incubated at 37°C. After the indicated time, plates were cooled on ice and all subsequent steps were performed on ice (Girard et al., 2005). Cells were washed three times with ice-cold F-F-54-30-II Buffer A (0.1 M MES pH 6.5, 1 mM EGTA, 0.5 mM $MgCl_2$, 1 mM PMSF, 1 μg/ml aprotinin, 1 μg/ml leupeptin, 1 μM pepstatin A, 1 mM DTT, 1 mM sodium orthovanadate and 5 mM NaF), scraped with a rubber policeman into Buffer A and dounce-homogenized (40 strokes with the tight pestle). The homogenate was centrifuged at 14,000 rpm in an F-54-30-II rotor for 20 minutes. The supernatant was further centrifuged at 38,000 rpm in an TLA-100.3 rotor for 1 hour. The pellet was resuspended in 500 μl Buffer A, loaded onto 3 ml of 8% sucrose in Buffer A and centrifuged at 35,000 rpm in a SW-55 Ti rotor: ***g*** for 2 hours. The pellet was either dissolved in sample buffer or solubilized, ultra-centrifuged and subjected to immunoprecipitation. The two methods resulted in an identical recovery of both CHC and other CCV-associated proteins (data not shown).

Internalization and recycling assays, and EGFR total surface levels

^{125}I-labelled EGF-internalization assays were performed as previously described (Innocenti et al., 2005). ^{125}I-labelled EGF (PerkinElmer) was 1.5 ng/ml (500 nCi/ml). Non-specific binding was measured for each time point in the presence of 100-fold molar excess of unlabeled EGF (PreproTech). Cells were serum starved and then incubated with ^{125}I-labelled EGF (1.5 ng/ml) for 2, 4 and 6 minutes at 37°C. The ratios of internalized and surface-bound (bound) radioactivity were determined and plotted over time. k_e values were derived as previously described (Wiley and Cunningham, 1982) using PRISM3 software. EGFR surface levels were measured with saturating amounts of ^{125}I-labelled EGF as previously described (Wiley and Cunningham, 1982). In the fluorescence-based assay, cell-surface EGFR was selectively marked by staining unpermeabilized cells with antibodies targeted against the ectodomain.

^{125}I-labelled EGF recycling assays were performed as follows: knockdown cells were plated into 24-well plates (100,000 cells per well). For each time point, four wells per knockdown were prepared. The day after, the cells were serum starved for 4 hours in basic buffer (DMEM with 0.1% BSA and 20 mM Hepes pH 7.4). Subsequently, the basic buffer was removed and either ice-cold binding buffer (DMEM with 0.1% BSA, 20 mM Hepes pH 7.4 and 2 ng/ml ^{125}I-labelled EGF) or ice-cold competition buffer (DMEM with 0.1% BSA, 20 mM Hepes pH 7.4, 2 ng/ml ^{125}I-labelled EGF and 200 ng/ml EGF) was added. A low dose of ^{125}I-labelled EGF (2 ng/ml) was used to specifically trigger CME of EGFR. The cells were incubated on ice for 1 hour under slow shaking. Cold medium was replaced with warm basic buffer and the cells were transferred to 37°C for 15 minutes. Afterwards, they were washed twice with ice-cold PBS and incubated with a mildly acidic salt wash buffer (0.2 M sodium acetate pH 4.5, 0.5 M NaCl) for 5 minutes on ice, followed by two washes with ice-cold binding buffer. ^{125}I-labelled EGF-loaded cells were chased in basic buffer supplemented with unlabeled EGF (400 ng/ml) at 37°C. At the end of each chase, the medium was collected and subjected to TCA precipitation to determine the amount of intact (TCA precipitable) and degraded (TCA soluble) ^{125}I-labelled EGF. Surface-bound ^{125}I-labelled EGF was extracted by acid treatment (0.2 M acetic acid pH 2.8, 0.5 M NaCl). Finally, cells were lysed in 1 M NaOH to determine the level of intracellular ^{125}I-labelled EGF. Recycled EGF was expressed as follows: intact ^{125}I-labelled EGF in the medium plus surface-bound ^{125}I-labelled EGF divided by the total (total medium plus total surface and total intracellular) after subtraction of the non-specific counts. Non-specific counts were measured for each time point and were never higher than 3–8% of the total counts.

Transfection and microscopy

Cells were seeded on gelatine-coated coverslips, transfected and processed for epifluorescence or indirect immunofluorescence microscopy as previously described (Beli et al., 2008). Wide-field micrographs were acquired as 16-bit images with a 63× (1.4 NA) oil objective and subsequently converted into 8-bit images with ImageJ. Confocal images were acquired using a Zeiss LSM510Meta set in the Multi-Track-acquisition mode with a 63× (1.4 NA) oil objective. Sections of 500 nm were taken along the *z*-axis. Representative central sections are shown. TIRF images were acquired using a Cell^R workstation (Olympus) equipped with 488 nm and 561 nm laser lines (both attenuated by 35%) and a PLAPO100xO/TIRFM-SP lens (1.45 NA). Incidence angles were set to achieve a penetration depth of 100 nm. Micrographs were captured as 16-bit images and subsequently converted into 8-bit images.

Phenotypic quantifications

Cell-surface EGFR levels were determined with ImageJ by measuring the average intensity of randomly selected regions of interest (ROIs). We quantified at least 40 cells (knockdown and rescued cells in Figs 4, 5 and 6), along with the neighbouring control cells, to derive average ROIs for a given sample. Mean values were always normalized with respect to the control (wild-type and non-transfected cells in Figs 4, 5 and 6). Similar results were obtained by visually determining the intensity of the anti-EGFR staining of the cell under scrutiny to the nearest controls within the same field (data not shown).

Association of F-actin with CCSs was evaluated on peripheral areas to minimize the scoring of clathrin-positive endosomes and vesicles, which are abundant in the cell centre. CCSs were considered phalloidin-positive when the F-actin staining was off-centred but overlapping, adjacent or centred with respect to CCSs. When the phalloidin signal associated with or adjacent to that of CHC did not differ from the background, CCSs were defined as F-actin-free (no actin). Only diffraction-limited CCSs were quantified. Blind counting of samples was performed in all instances.

Actin polymerization assays

The assay was performed as previously described (Innocenti et al., 2005). The final concentrations of Arp2/3 complex, G-actin, pyrenyl-actin, GST–VCA, GST–N-WASP, CK2α, CK2β and Cdc42 were 0.02, 2, 0.5, 0.25, 0.015, 1, 1 and 1 μM, respectively. Cdc42 production and loading were performed as previously described (Innocenti et al., 2005). Purified bovine Arp2/3 complex, muscle and pyrene-labeled actin were from Cytoskeleton Inc. Actins were recycled prior to use (Hertzog and Carlier, 2005). In all cases, one of the three experiments that were performed with similar results is shown. Storage of CK2α and CK2α K68A resulted in a progressive loss of their N-WASP-inhibiting activities accompanied with partial degradation. To minimize this, CK2α and CK2α K68A were tested within 2 weeks of purification. The concentration of barbed ends ([F]) was derived from the rate of growth (V) using the equation $V=k_+$ [F] (C–C_c), where k_+ is the association rate constant (10 $\mu M^{-1}s^{-1}$), C the concentration of G-actin at mid-polymerization (1.25 μM) and C_c is the critical concentration (0.1 μM).

Gel filtration

Lysates were prepared in buffer L (50 mM HEPES pH 7.5, 1% glycerol, 150 mM NaCl, 1% Triton X-100, 1.5 mM $MgCl_2$, 5 mM EGTA, and protease and phosphatase inhibitors). After ultracentrifugation (23,000 rpm in a TLA-100.3 rotor for 30 minutes at 4°C), 1.5 mg lysate was loaded onto a Superose 6 10/300 GL column (GE Healthcare), pre-equilibrated in buffer GF (50 mM HEPES pH 7.5, 1% glycerol, 150 mM NaCl, 1.5 mM $MgCl_2$, 5 mM EGTA, and protease and phosphatase inhibitors). Gel filtration was performed at 4°C in buffer B at a flow rate of 0.5 ml/minute and fractions of 500 μl were collected.

Densitometry

Eight-bit scans were analysed with Quantity One, as previously described (Beli et al., 2008). Multiple and preferably non-saturated exposures of the same blot were quantified and data averaged in all cases.

DMAT treatment

DMAT was dissolved in DMSO at a concentration of 20 mM. Cells were incubated with DMAT (50 μM) for 3 hours to achieve CK2 inhibition. Control cells were mock-treated by adding an equivalent volume of DMSO. Under these conditions, CK2 activity was efficiently inhibited (data not shown).

Statistics

Unless indicated, data are expressed as the means±s.d. for at least three independent experiments. Two-sided two-sample *t*-tests or appropriate ANOVA tests were performed.

We thank E. Haugsten, T. Scanu and Y. Goldberg for reagents, Marie-France Carlier for help with the actin polymerization assays, the NKI Protein facility for gel filtrations and E. Argenzio for drawing Fig. 8. D.X. was supported by a long-term fellowship from the Human Frontier Science Program. M.G. performed experiments and analysed data in Fig. 2B–D, Fig. 3C, Fig. 4A,B, supplementary material Fig. S1F,G, supplementary material Fig. S3A,B, supplementary material Fig. S4A, supplementary material Fig. S5E, supplementary material Fig. S6C,E, and supplementary material Fig. S7. M.G. prepared reagents used in Fig. 3 and performed experiments in Fig. 5A,B. D.X. performed experiments and analysed data in Fig. 1D,E, Fig. 2A,E,F, Fig. 4B–D, Fig. 5D,E, Fig. 6, supplementary material Fig. S1A,C,E, supplementary material Fig. S5B–G, supplementary material Fig. S6D.

L.B.A. performed the MS analysis identifying CK2 as an N-WASP-interacting protein. R.v.d.K. prepared reagents in Fig. 3 and provided technical support. M.I. conceived and directed the project, performed experiments and analysed data. M.I. wrote the manuscript.

Supplementary material available online at
http://jcs.biologists.org/cgi/content/full/124/12/2001/DC1

References

Arrigoni, G., Pagano, M. A., Sarno, S., Cesaro, L., James, P. and Pinna, L. A. (2008). Mass spectrometry analysis of a protein kinase CK2beta subunit interactome isolated from mouse brain by affinity chromatography. *J. Proteome Res.* **7**, 990-1000.

Bar-Zvi, D. and Branton, D. (1986). Clathrin-coated vesicles contain two protein kinase activities. Phosphorylation of clathrin beta-light chain by casein kinase II. *J. Biol. Chem.* **261**, 9614-9621.

Beli, P., Mascheroni, D., Xu, D. and Innocenti, M. (2008). WAVE and Arp2/3 jointly inhibit filopodium formation by entering into a complex with mDia2. *Nat. Cell Biol.* **10**, 849-857.

Benesch, S., Polo, S., Lai, F. P., Anderson, K. I., Stradal, T. E., Wehland, J. and Rottner, K. (2005). N-WASP deficiency impairs EGF internalization and actin assembly at clathrin-coated pits. *J. Cell Sci.* **118**, 3103-3115.

Bibby, A. C. and Litchfield, D. W. (2005). The multiple personalities of the regulatory subunit of protein kinase CK2: CK2 dependent and CK2 independent roles reveal a secret identity for CK2beta. *Int. J. Biol. Sci.* **1**, 67-79.

Bolte, S. and Cordelieres, F. P. (2006). A guided tour into subcellular colocalization analysis in light microscopy. *J. Microsc.* **224**, 213-232.

Cheng, H. C., Skehan, B. M., Campellone, K. G., Leong, J. M. and Rosen, M. K. (2008). Structural mechanism of WASP activation by the enterohaemorrhagic E. coli effector EspF(U). *Nature* **454**, 1009-1013.

Conner, S. D. and Schmid, S. L. (2003). Regulated portals of entry into the cell. *Nature* **422**, 37-44.

Cory, G. O., Cramer, R., Blanchoin, L. and Ridley, A. J. (2003). Phosphorylation of the WASP-VCA domain increases its affinity for the Arp2/3 complex and enhances actin polymerization by WASP. *Mol. Cell* **11**, 1229-1239.

Ehrlich, M., Boll, W., Van Oijen, A., Hariharan, R., Chandran, K., Nibert, M. L. and Kirchhausen, T. (2004). Endocytosis by random initiation and stabilization of clathrin-coated pits. *Cell* **118**, 591-605.

Ferguson, S., Raimondi, A., Paradise, S., Shen, H., Mesaki, K., Ferguson, A., Destaing, O., Ko, G., Takasaki, J., Cremona, O. et al. (2009). Coordinated actions of actin and BAR proteins upstream of dynamin at endocytic clathrin-coated pits. *Dev. Cell* **17**, 811-822.

Girard, M., Allaire, P. D., Blondeau, F. and McPherson, P. S. (2005). Isolation of clathrin-coated vesicles by differential and density gradient centrifugation. *Curr. Protoc. Cell Biol.* **Chapter 3**, Unit 3.13.

Hertzog, M. and Carlier, M. F. (2005). Functional characterization of proteins regulating actin assembly. *Curr. Protoc. Cell Biol.* **Chapter 13**, Unit 13.6.

Innocenti, M., Zucconi, A., Disanza, A., Frittoli, E., Areces, L. B., Steffen, A., Stradal, T. E., Di Fiore, P. P., Carlier, M. F. and Scita, G. (2004). Abi1 is essential for the formation and activation of a WAVE2 signalling complex. *Nat. Cell Biol.* **6**, 319-327.

Innocenti, M., Gerboth, S., Rottner, K., Lai, F. P., Hertzog, M., Stradal, T. E., Frittoli, E., Didry, D., Polo, S., Disanza, A. et al. (2005). Abi1 regulates the activity of N-WASP and WAVE in distinct actin-based processes. *Nat. Cell Biol.* **7**, 969-976.

Jiang, X., Huang, F., Marusyk, A. and Sorkin, A. (2003). Grb2 regulates internalization of EGF receptors through clathrin-coated pits. *Mol. Biol. Cell* **14**, 858-870.

Kaksonen, M., Toret, C. P. and Drubin, D. G. (2006). Harnessing actin dynamics for clathrin-mediated endocytosis. *Nat. Rev. Mol. Cell Biol.* **7**, 404-414.

Kim, A. S., Kakalis, L. T., Abdul-Manan, N., Liu, G. A. and Rosen, M. K. (2000). Autoinhibition and activation mechanisms of the Wiskott-Aldrich syndrome protein. *Nature* **404**, 151-158.

Kirchhausen, T. (2000). Clathrin. *Annu. Rev. Biochem.* **69**, 699-727.

Korolchuk, V. I. and Banting, G. (2002). CK2 and GAK/auxilin2 are major protein kinases in clathrin-coated vesicles. *Traffic* **3**, 428-439.

Korolchuk, V. and Banting, G. (2003). Kinases in clathrin-mediated endocytosis. *Biochem. Soc. Trans.* **31**, 857-860.

Lamaze, C., Fujimoto, L. M., Yin, H. L. and Schmid, S. L. (1997). The actin cytoskeleton is required for receptor-mediated endocytosis in mammalian cells. *J. Biol. Chem.* **272**, 20332-20335.

Meggio, F. and Pinna, L. A. (2003). One-thousand-and-one substrates of protein kinase CK2? *FASEB J.* **17**, 349-368.

Merrifield, C. J., Qualmann, B., Kessels, M. M. and Almers, W. (2004). Neural Wiskott Aldrich Syndrome Protein (N-WASP) and the Arp2/3 complex are recruited to sites of clathrin-mediated endocytosis in cultured fibroblasts. *Eur. J. Cell Biol.* **83**, 13-18.

Merrifield, C. J., Perrais, D. and Zenisek, D. (2005). Coupling between clathrin-coated-pit invagination, cortactin recruitment, and membrane scission observed in live cells. *Cell* **121**, 593-606.

Pagano, M. A., Meggio, F., Ruzzene, M., Andrzejewska, M., Kazimierczuk, Z. and Pinna, L. A. (2004). 2-Dimethylamino-4,5,6,7-tetrabromo-1H-benzimidazole: a novel powerful and selective inhibitor of protein kinase CK2. *Biochem. Biophys. Res. Commun.* **321**, 1040-1044.

Perrais, D. and Merrifield, C. J. (2005). Dynamics of endocytic vesicle creation. *Dev. Cell* **9**, 581-592.

Prehoda, K. E., Scott, J. A., Mullins, R. D. and Lim, W. A. (2000). Integration of multiple signals through cooperative regulation of the N-WASP-Arp2/3 complex. *Science* **290**, 801-806.

Puri, C., Tosoni, D., Comai, R., Rabellino, A., Segat, D., Caneva, F., Luzzi, P., Di Fiore, P. P. and Tacchetti, C. (2005). Relationships between EGFR signaling-competent and endocytosis-competent membrane microdomains. *Mol. Biol. Cell* **16**, 2704-2718.

Riedl, J., Crevenna, A. H., Kessenbrock, K., Yu, J. H., Neukirchen, D., Bista, M., Bradke, F., Jenne, D., Holak, T. A., Werb, Z. et al. (2008). Lifeact: a versatile marker to visualize F-actin. *Nat. Methods* **5**, 605-607.

Sallee, N. A., Rivera, G. M., Dueber, J. E., Vasilescu, D., Mullins, R. D., Mayer, B. J. and Lim, W. A. (2008). The pathogen protein EspF(U) hijacks actin polymerization using mimicry and multivalency. *Nature* **454**, 1005-1008.

Sigismund, S., Woelk, T., Puri, C., Maspero, E., Tacchetti, C., Transidico, P., Di Fiore, P. P. and Polo, S. (2005). Clathrin-independent endocytosis of ubiquitinated cargos. *Proc. Natl. Acad. Sci. USA* **102**, 2760-2765.

Sorkin, A. and Goh, L. K. (2008). Endocytosis and intracellular trafficking of ErbBs. *Exp. Cell Res.* **314**, 3093-3106.

Takenawa, T. and Suetsugu, S. (2007). The WASP-WAVE protein network: connecting the membrane to the cytoskeleton. *Nat. Rev. Mol. Cell Biol.* **8**, 37-48.

Ungewickell, E. J. and Hinrichsen, L. (2007). Endocytosis: clathrin-mediated membrane budding. *Curr. Opin. Cell Biol.* **19**, 417-425.

Wiley, H. S. and Cunningham, D. D. (1982). The endocytotic rate constant. A cellular parameter for quantitating receptor-mediated endocytosis. *J. Biol. Chem.* **257**, 4222-4229.

Yarar, D., Waterman-Storer, C. M. and Schmid, S. L. (2005). A dynamic actin cytoskeleton functions at multiple stages of clathrin-mediated endocytosis. *Mol. Biol. Cell* **16**, 964-975.